$Ad5_{NULL}$-A20 – a tropism-modified, αvβ6 integrin-selective oncolytic adenovirus for epithelial ovarian cancer therapies

Running title: $Ad5_{NULL}$-A20: an exquisitely tumour-selective virotherapy

Hanni Uusi-Kerttula[1], James A. Davies[1], Jill M. Thompson[2], Phonphimon Wongthida[2], Laura Evgin[2], Kevin G. Shim[2], Angela Bradshaw[3], Alexander T. Baker[1], Pierre J. Rizkallah[4], Rachel Jones[5], Louise Hanna[6], Emma Hudson[6], Richard G. Vile[2], John D. Chester[1,6], Alan L. Parker[1]*

[1] Division of Cancer and Genetics, Cardiff University, Cardiff CF14 4XN, United Kingdom

[2] Department of Molecular Medicine, Mayo Clinic, Rochester, MN 55905, United States

[3] BHF Glasgow Cardiovascular Research Centre, Glasgow G12 8TA, United Kingdom

[4] Division of Infection and Immunity, Cardiff University, Cardiff CF14 4XN, United Kingdom

[5] South West Wales Cancer Institute, Singleton Hospital, Swansea SA2 8QA, United Kingdom

[6] Velindre Cancer Centre, Cardiff CF14 2TL, United Kingdom

*** Corresponding author**

Dr Alan L. Parker
Division of Cancer and Genetics
Henry Wellcome Building
Cardiff University School of Medicine
Heath Park
Cardiff
CF14 4XN
Email: parkeral@cardiff.ac.uk
Tel: 02922510231

Conflict of interest: None of the authors declare conflict of interest.

Keywords: oncolytic adenovirus, αvβ6 integrin, re-targeting, epithelial ovarian cancer
Word count: 3333 words (excluding Figure legends)
Abstract: 250 words

Figure count: 7 + Supplementary Methods + 4 Supplementary Figures

Translational relevance:

Virotherapies are emerging as clinically important anticancer agents, demonstrating synergy with immune checkpoint inhibitors in several recent, high profile studies. Since these agents have not evolved to be intrinsically tumour selective, therapeutic index could be further enhanced by a thorough redesign of the virus capsid to improve tumour selectivity following intravascular delivery. To this end, we have systematically refined the adenovirus serotype 5 (Ad5) capsid to genetically preclude uptake via all known native cellular entry pathways, to generate a basal and more biocompatible vector, $Ad5_{NULL}$. To empower this vector with tumour selectivity, we further engineered the $Ad5_{NULL}$ capsid to present a high-affinity αvβ6 integrin-binding oligopeptide, A20. The resultant virotherapy, $Ad5_{NULL}$-A20 demonstrates exquisite tumour-selectivity both in vitro and in vivo, with basal "off-target" uptake. $Ad5_{NULL}$-A20 thus represents a powerful platform for targeted in situ over-expression of immunomodulatory modalities for future translational applications.

Abbreviations:

A20, a 20-amino acid peptide NAVPNLRGDLQVLAQKVART
Ad5, adenovirus serotype 5
CAR, coxsackie and adenovirus receptor
EOC, epithelial ovarian cancer
FMDV, foot-and-mouth disease virus
FX, coagulation factor 10
OAS, ovarian ascites

ABSTRACT

Purpose:

Virotherapies are maturing in the clinical setting. Adenoviruses (Ad) are excellent vectors for manipulability and tolerance of transgenes. Poor tumour-selectivity, off-target sequestration and immune inactivation hamper clinical efficacy. We sought to completely redesign Ad5 into a refined, tumour selective virotherapy targeted to αvβ6 integrin, which is expressed in a range of aggressively transformed epithelial cancers but non-detectable in healthy tissues.

Experimental Design:

$Ad5_{NULL}$-A20 harbours mutations in each major capsid protein to preclude uptake via all native pathways. Tumour-tropism via αvβ6-targeting was achieved by genetic insertion of A20 peptide (NAVPNL**RGD**LQVLAQKVART) within the fiber knob protein. The vector's selectivity in vitro and in vivo was assessed.

Results:

The tropism-ablating triple mutation completely blocked all native cell entry pathways of $Ad5_{NULL}$-A20 via coxsackie and adenovirus receptor (CAR), αvβ3/5 integrins and coagulation factor 10 (FX). $Ad5_{NULL}$-A20 efficiently and selectively transduced αvβ6+ cell lines and primary clinical ascites-derived EOC ex vivo, including in the presence of pre-existing anti-Ad5 immunity. In vivo biodistribution of $Ad5_{NULL}$-A20 following systemic delivery in non-tumour-bearing mice was significantly reduced in all off-target organs, including a remarkable 10^7-fold reduced genome accumulation in the liver compared to Ad5. Tumour uptake, transgene expression and efficacy were confirmed in a peritoneal SKOV3 xenograft model of human EOC, where oncolytic $Ad5_{NULL}$-A20-treated animals demonstrated significantly improved survival compared to those treated with oncolytic Ad5.

Conclusions:

Oncolytic $Ad5_{NULL}$-A20 virotherapies represent an excellent vector for local and systemic targeting of αvβ6-over-expressing cancers, and exciting platforms for tumour selective over-expression of therapeutic anti-cancer modalities, including immune checkpoint inhibitors.

INTRODUCTION

Ovarian cancer remains the deadliest gynaecological cancer with global 5-year survival rates below 50% (1). The early stages of the disease are commonly asymptomatic, with the result that most patients have advanced, incurable disease, at presentation. Ovarian cancer metastasises with large volumes of malignant, intraperitoneal ovarian ascites (OAS) providing a pro-tumourigenic microenvironment (2). Chemo-resistance rapidly develops during treatment, requiring alternative regimens. Epithelial ovarian cancer (EOC) is the most common (90%) ovarian cancer type (3). A third of EOC patients have cells expressing an epithelial cancer-specific marker, αvβ6 integrin (4). Upregulation of αvβ6 expression in cancer has been linked to aggressive transformation, metastasis and poor prognosis (5-8). αvβ6 is absent in healthy epithelium (5, 9) but widely over-expressed in plethora of cancers, including ovarian, lung, skin, oesophageal, cervical, and head and neck cancer (4), thus making it a promising target for therapeutic vectors. αvβ6 is an activator of TGF-β1 signalling that promotes metastasis by enhancing angiogenesis, immune cell suppression and epithelial-to-mesenchymal transition [reviewed in (10)].

Cancer virotherapy is undergoing renewed interest, including recent regulatory approval for clinical use of herpes simplex type 1-based talimogene laherparepvec (T-VEC), the first oncolytic immunotherapy approved for advanced melanoma (11). Very recently oncolytic viruses were shown to sensitise difficult-to-treat tumours, including triple-negative breast cancer (TNBC) (12) and glioblastoma (13) to subsequent immunotherapies with immune checkpoint inhibitors. This highlights the potential of virotherapies for combination studies in the clinical setting, and the scope for generating a vector capable of systemically targeting tumours following intravenous introduction. Adenovirus serotype 5 (Ad5) has been commonly deployed in clinical trials of cancer and gene therapies (14), due to ease of genetic manipulation and capacity for large transgenes (15). However, this serotype has sub-optimal features that hamper its wider clinical use. As a common respiratory virus with high seroprevalence rates (16), efficient neutralisation of vector by neutralising antibodies

(nAbs) limits efficacy. Other limitations include significant and rapid off-target sequestration to spleen and liver via complexing of the virion with human coagulation factor 10 (FX) (17) and potentially other coagulation factors [reviewed extensively in (18)], "bridging" the complex to heparan sulphate proteoglycans (HSPGs), abundant on hepatocytes (19). In vitro, Ad5 enters host cells via coxsackie and adenovirus receptor (CAR) (20) that is ubiquitous within tight junctions on polarised epithelial cells [reviewed in (21)] but commonly down-regulated in progressive cancers (22-26), limiting use of wild-type Ad5 for tumour therapy.

We have generated a novel virotherapy vector, $Ad5_{NULL}$-A20, with altered, tumour-selective tropism. We ablated all native tropisms of Ad5 by mutating key residues in the three main capsid proteins (hexon, fiber and penton) and re-targeted the resulting vector, $Ad5_{NULL}$, to the tumour-selective integrin αvβ6 through incorporation of an αvβ6-binding peptide (A20, NAVPNL**RGD**LQVLAQKVART) within the fiber knob domain HI loop, generating the novel vector $Ad5_{NULL}$-A20. A20 peptide was originally derived from foot-and-mouth disease virus (FMDV) capsid protein VP1, and has high affinity for its native receptor, αvβ6 integrin (27, 28). We have investigated potential clinical utility of an oncolytic variant of $Ad5_{NULL}$-A20 (Δ24/T1) for intra-peritoneal treatment of ovarian cancer by investigating its bio-distribution, tumour-selective oncolytic capabilities and avoidance of immune neutralisation using in vitro and in vivo models of human EOC.

MATERIALS AND METHODS

Adenovirus vectors, cell lines and clinical ascites

All vectors generated in this study included a luciferase (Luc) reporter gene. Genetic modifications were carried out by AdZ homologous recombineering methods (29) as described previously (30). Viruses were produced in T-REx-293 or HEK293-β6 cells (for A20-modified viruses) and purified as described previously (30, 31). A triply de-targeted vector genome, $Ad5_{NULL}$, was generated by introducing mutations in key genes encoding of

each of the major capsid proteins to preclude cellular uptake by all known native Ad5 pathways. Ablation of binding to CAR was achieved via the KO1 mutation in the AB loop of the L5 fiber knob gene; ablation of binding to coagulation factor 10 (FX) via a mutation in hypervariable region 7 of the L3 hexon gene; and ablation of αvβ3/5 integrin binding via RGD-to-RGE mutation in the L2 penton base gene. αvβ6 re-targeting was achieved by insertion of sequences encoding peptide A20 (NAVPNL**RGD**LQVLAQKVART) into the fiber knob HI loop (between residues G546 and D547) of $Ad5_{NULL}$, generating $Ad5_{NULL}$-A20. Replication-deficient variants of $Ad5_{NULL}$-A20 carry a complete E1/E3 deletion. Oncolytic variants have a 24-base pair deletion (dl922–947) in the retinoblastoma protein (pRB) binding domain of E1A (Δ24) (32) and a single adenine insertion at position 445 within the endoplasmic reticulum (ER) retention domain of E3/19K [T1 mutation; (33)]. Additional details of genetic modifications are provided in Supplementary Methods.

Homology modelling was performed using the previously published Ad5 fiber knob structure [PDB ID: 1KNB (34)] and foot-and-mouth disease virus O PanAsia VP1 protein in complex with αvβ6 [PDB ID: 5NEM (35)]. The peptide sequence forming the interaction with αvβ6 (NVRGDLQVLAQKVART) was edited to conform with the A20 peptide sequence used in this study (NAVPNLRGDLQVLAQKVART), docked to the Ad5 fiber knob structure in the HI loop and the KO1 mutation added using WinCoot (36) and PyMol 2.0 (37). The crude $Ad5_{NULL}$-A20 structure was aligned with the existing 5NEM structure and the complex energy minimised using the YASARA algorithm (38). Binding energy calculations were performed using PISA (39), and surface charge calculated using APBS tool in PyMol 2.0 (37).

αvβ6-high/CAR+ SKOV3-β6 cell line was generated in-house by retroviral transfection of SKOV3 cells [that natively express the αv subunit (40)] with integrin beta6 pBABE puro plasmid to express the β6 subunit. Primary EOC cells from ascites were obtained through Wales Cancer Bank under existing ethical permissions (WCB 14/004). Cells were processed and sub-cultured as described previously (30, 31), and tested regularly for Mycoplasma infection by commercially available PCR-based methods.

In vitro and in vivo studies

Cell surface receptor expression was assessed by flow cytometry (30). The presence of anti Ad5 antibodies in ovarian ascites and serum was determined by ELISA as previously reported (41). Antigen specificity of the antibodies was assessed by Western blot. Transduction efficiency was assessed by standard luciferase assays, described previously (30, 31). Animal experiments were approved by Institutional Care and Use Committee (IACUC) and performed at Mayo Clinic, Rochester, MN, USA. Animals were age and sex-matched. Animal handling and injections were performed by a veterinary technologist. In vivo experiments are further described in detail in Supplementary Methods.

Statistical analyses

Figures and statistical analyses were generated using GraphPad Prism v6.03. In vitro and ex vivo assays were analysed by two-tailed unpaired t-tests or one-way ANOVA with Dunnett's multiple comparisons post hoc test. In vivo data was normalised and analysed by one-way ANOVA or Kruskal–Wallis test with Sidak's or Dunn's multiple comparisons post hoc test, respectively. Overall survival (%) following oncolytic treatment is shown as a Kaplan–Meier survival curve; survival proportions were analysed by Gehan–Breslow–Wilcoxon test.

RESULTS

We generated and produced to very high viral titres replication-defective and oncolytic variants of a novel $Ad5_{NULL}$-A20 vector (Fig. 1A) with three de-targeting mutations and an A20 peptide insertion that re-targets the vector to αvβ6 integrin-expressing cells (Fig. 1B). Additionally, we generated replication deficient and oncolytic versions of Ad5.A20, which harbours the αvβ6 targeting-peptide A20 insertion, in the absence of any de-targeting modification. The multiple genetic manipulations did not have a significant impact on viral titre (Fig. 1A).

We generated a homology model of the $Ad5_{NULL}$-A20 fiber knob protein in complex with the αvβ6 dimer (Fig. 1C). The A20 peptide (dark blue) occupies space spanning both αv (green) and β6 (purple) subunits. The predicted $Ad5_{NULL}$-A20 interacting residues of the A20 peptide (dark blue) and the native knob structure (cyan) against the approximated charge surface of the αvβ6 (red is negative, blue is positive, Fig. 1D). The αvβ6 has mostly negative surface potential in this region (1D), complementary to the predominantly positive charge of the $Ad5_{NULL}$-A20 interface (Suppl. Fig. I A). The adjacent CD loop of the native Ad5 fiber knob contributes two polar residue interactions from Lys-442 and Gly-443 (1D), binding to an additional three αv residues (Suppl. Fig. I B). The binding energy of the αvβ6-$Ad5_{NULL}$-A20 fiber knob complex is calculated to be –24.3 $Kcalmol^{-1}$, suggesting an exceptionally stable interface (Suppl. Fig. I C), providing confidence that our αvβ6 targeting strategy was feasible.

The transduction efficiency of replication-deficient vectors was assessed in cell lines expressing variable levels of CAR and αvβ6 integrin. The de-targeting mutation triplet of $Ad5_{NULL}$-A20 completely abolished entry via CAR in CHO-CAR cells (CAR+), while Ad5 transduced these cells at expectedly high efficiency (Fig. 2A). The HVR7 mutation abolished Ad5 vector transduction via FX pathway (Fig. 2B) (42). As expected, FX significantly increased transduction of Ad5 into CHO-K1 cells as compared to FX-free culture conditions (Fig. 2B; left panel). Conversely, addition of human FX in culture medium had no effect on the transduction efficiency of the FX binding-ablated Ad5.HVR7 control vector in these cells (Fig. 2B; right panel). Furthermore, the enhanced transduction seen for Ad5 was reversed by the addition of a 3:1 molar excess of Gla-domain interacting protein, anticoagulant X-bp, that binds and inactivates FX in the medium (19) (Fig. 2B, left panel). On the contrary, FX depletion did not affect the transduction of Ad5.HVR7 vector (Fig. 2B, right panel).

We confirmed αvβ6 integrin as the primary entry receptor for the triply de-targeted, integrin re-targeted $Ad5_{NULL}$-A20 vector (Fig. 3). $Ad5_{NULL}$-A20 transduced αvβ6+/CAR– BT-20 breast cancer cells with 305-fold higher efficiency (Fig. 3A; $p=0.0270$) and primary, patient

derived EOC004 cells (αvβ6+/CAR–) at 69-fold increased efficiency (Fig. 3B; p=0.0090) relative to Ad5. Competition assays using a function-blocking anti-αvβ6 antibody (10D5) significantly inhibited cell transduction by $Ad5_{NULL}$-A20 vector in SKOV3-β6 cells (αvβ6+/CAR+) (Fig. 3C; p=0.0010), confirming the vector's selectivity for αvβ6 integrin

We next evaluated the ability of the $Ad5_{NULL}$-A20 vector to retain its infectivity in the highly neutralising environment presented by ovarian ascites. To this end, freshly isolated clinical OAS samples from twenty ovarian cancer patients were screened for the presence of anti-Ad5 antibodies by direct ELISA. The titres of anti-Ad5 abs in malignant ovarian ascites were scrutinised against the serum anti-Ad5 antibody titre of a healthy adult male volunteer (Fig. 4A). Equal proportion of patients were found to have lower and higher antibody titres than the control serum (Fig. 4A, black dashed line). Ascites from patient 001 (OAS001) was chosen for subsequent neutralisation assays due to its similar antibody titre with the control serum. Antibodies in OAS001 and control serum appeared specific for the viral fiber protein, whilst the most abundant capsid protein – hexon – was recognised only at very low levels in Western blot using denatured whole viral particles (Fig. 4B). The neutralising effect of OAS001 on transduction efficiency of $Ad5_{NULL}$-A20 was assessed in αvβ6+/CAR– EOC004 primary cells. $Ad5_{NULL}$-A20 showed up to 902-fold higher transduction efficiency in primary human EOC cultures relative to Ad5 at OAS concentrations of 2.5, 5 and 10%, whilst Ad5 was not capable of transducing these cells at detectable levels (Fig. 4C).

We next evaluated biodistribution of virus infection in immunocompetent, non-tumour-bearing mice. Mice were injected intravenously with replication-defective vectors to assess in vivo tropism (Fig. 5A), in particular the effect of the three de-targeting mutations on biodistribution of virus infection. As expected and as previously documented, the Ad5 vector showed intense localisation in the area of liver and spleen, while luminescence by the $Ad5_{NULL}$-A20 vector was completely undetectable at the 72-h time-point (Fig. 5B). Animals inoculated with Ad5 vector had significantly higher whole-body luminescence than the control animals ($p<0.0001$) or the $Ad5_{NULL}$-A20 vector ($p<0.0001$) (Fig. 5C). The liver, spleen,

lungs, ovaries and heart were resected post-mortem and quantified for ex vivo luminescence (for luminescence heat-maps, see Suppl. Fig. II A–C). The livers of Ad5-challenged animals emitted significantly more luminescence than the PBS control or $Ad5_{NULL}$-A20 groups (both $p<0.0001$) (Fig. 5D). Similarly, $Ad5_{NULL}$-A20 had significantly decreased transgene expression in the spleen, lungs, ovaries and heart, relative to Ad5 (Fig. 5E–H; $p<0.0001$ for all). For fold changes in luminescence intensity in each off-target organ, see Suppl. Fig. II D.

Confirmation that the modifications in $Ad5_{NULL}$-A20 resulted in reduced sequestration of virus in multiple normal tissues was performed via quantitation of viral load by qPCR. Genome copy number of the $Ad5_{NULL}$-A20 vector was 10 million times lower in the liver relative to the Ad5 (Fig. 6A; $p<0.0001$). Similarly, $Ad5_{NULL}$-A20 genome copy number was over 700-fold lower in the spleen compared to Ad5 (Fig. 6B; $p<0.0001$). In addition, the $Ad5_{NULL}$-A20 vector showed improved off-target profiles in all organs relative to Ad5, with viral load 10^5, 10^4 and 10^3 lower in the lungs, heart and ovaries, respectively (Fig. 6C–E). Successful de-targeting of the liver being due to our genetic modifications of Ad5 is supported by immunohistochemical staining of liver sections, which showed high expression levels of CAR, whilst αvβ6 was undetectable (Suppl. Fig. III A). Confirmation of the de-targeting effects of genetic modifications in $Ad5_{NULL}$-A20 is provided by the observation that liver sections from mice showed positive staining for Ad capsid proteins in the Ad5 group, but not in livers of mice that had been challenged with the $Ad5_{NULL}$-A20 vector (Suppl. Fig. III B).

To evaluate efficacy in a human EOC model in vivo, SKOV3 human ovarian cancer xenografts were established in immuno-compromised NOD/SCID mice. Animals developed large solid tumours at the cell injection site and at various sites within the peritoneal cavity within 14 days after intra-peritoneal implantation of SKOV3 cells (for tumour localisation and take rate, see Suppl. Fig. IV) and by day 49, tumours were spread throughout the peritoneal cavity with accumulation of large volumes of ascites. Based on these observations, we performed virotherapy efficacy studies by delivering three intraperitoneal doses of oncolytic

278 variants of Ad5, Ad5.A20 and $Ad5_{NULL}$-A20 vectors on days 14, 16 and 18 post-implantation
279 of SKOV3 cells.

280 IVIS imaging at 48 h after first virotherapy treatment dose (day 16) showed widespread
281 luminescence throughout the abdominal region in animals with SKOV3 xenografts and
282 treated with the oncolytic Ad5 vector, with highest intensity in the liver/spleen region (Fig.
283 7B). This distribution was maintained, but at lower intensity, until 5 days later, day 21 (Fig.
284 7B). In contrast, the oncolytic $Ad5_{NULL}$-A20 vector however, showed selective tumour
285 localisation, with significantly reduced overall luminescence relative to Ad5, consistent with
286 successful de-targeting of non-tumour tissues. The distribution of infection mediated by the
287 oncolytic Ad5.A20 vector was intermediate between the Ad5 and $Ad5_{NULL}$-A20. Quantitation
288 of total body luminescence showed uptake of the $Ad5_{NULL}$-A20 vector to be significantly lower
289 than Ad5 both on day 16 (Fig 7C; $p<0.05$ and <0.01, respectively) and on day 21 (Fig. 7D;
290 $p<0.0001$), while there was no statistically significant difference in the uptake of Ad5.A20 as
291 compared to Ad5.

292 Anti-tumour activity was observed for oncolytic Ad5, oncolytic Ad5.A20 and oncolytic
293 $Ad5_{NULL}$-A20 in the SKOV3 xenograft model (Fig 7E). Consistent with an enhanced tumour-
294 selective effect of $Ad5_{NULL}$-A20, all mice treated with $Ad5_{NULL}$-A20 were still alive and tumour-
295 free at the final time-point of 101 days, while animals treated with either Ad5 or Ad5.A20
296 almost identical (and statistically not significantly different) survival curves with median
297 survival of around 60 days.

298

DISCUSSION

We describe here an exquisitely refined and tumour-selective oncolytic adenoviral vector, $Ad5_{NULL}$-A20 which is ablated for all known native tropisms and re-targeted to an over-expressed, prognostic cancer marker – αvβ6 integrin (43). Integrin αvβ6 is a promising target for therapeutic cancer applications due to its over-expression in aggressively transformed cancers (4). A20 peptide is a feasible tool for a variety of clinical applications, and has been used for imaging diagnostics in an αvβ6+ pancreatic tumour model (44) and in a humanised single-chain Fv antibody B6-2 (45). αvβ6 is emerging as a promising target for a range of advances therapies including those based on chimaeric antigen receptor (CAR) T-cell immunotherapies [reviewed in (46)], where efficacy in the αvβ6 expressing SKOV3 cell lines has been demonstrated. Furthermore, the αvβ6-blocking antibody, 264RAD showed promising in vivo efficacy in HER2+/αvβ6+ breast cancers in combination with monoclonal antibody trastuzumab (47), and is being developed for phase I clinical trials. αvβ6 therefore represents a highly appealing target for cancer treatment across a range of technologies and therapeutic applications.

In silico evaluation of the $Ad5_{NULL}$-A20 interface with αvβ6 by homology modelling (Fig. 1; Suppl. Fig. I) predicts the $Ad5_{NULL}$-A20 fiber knob domain to form a low entropy interface with αvβ6. A20 possesses the putative RGD integrin interacting motif (48) but specificity to the β6 subunit is derived from the helical motif C-terminal of RGD. It is further stabilised by electrostatic interactions across the interface and polar bonds between αv and the Ad5 CD loop. Each fiber trimer possesses three copies of the A20 peptide, with 12 trimeric fibers per adenovirus capsid, thus $Ad5_{NULL}$-A20 possesses 36 potential αvβ6 interaction sites per viral particle. While not all these sites will be utilised in a single cellular interaction it is extremely likely that the virus benefits from a potent avidity effect when interacting with a cell possessing multiple αvβ6 copies.

In the present study, we presented the $Ad5_{NULL}$-A20 as a highly selective vector platform. A replication-defective form of $Ad5_{NULL}$-A20 vector successfully de-targeted viral

uptake by cells via native viral uptake pathways (Fig. 2), instead selectively re-targeting αvβ6+ cells, in vitro and ex vivo (Fig. 3). Although the efficacy-limiting interactions that occur in systemic delivery of adenoviral vectors can, theoretically, be bypassed by intra-cavity administration of the vector via the i.p. route, in practice this approach presents challenges since wild-type Ad5 is sequestered by pre-existing anti-Ad5 immunity in the form of neutralising antibodies (nAbs) in ascitic fluid (41, 49, 50). We therefore assessed the transduction efficiency of $Ad5_{NULL}$-A20 in the presence of freshly-isolated clinical OAS from ovarian cancer patients with confirmed high levels of anti-Ad5 nAbs (Fig. 4A). Unlike the Ad5 vector, $Ad5_{NULL}$-A20 retained its ability to transduce αvβ6+ cells, even at relatively high OAS concentrations (Fig. 4C).

Clinical efficacy of therapeutic Ad5 vectors with unmodified capsids is also significantly limited by off-target tissue sequestration, particularly in the liver. We demonstrate that $Ad5_{NULL}$-A20 significantly altered the biodistribution of the Ad5 vector in vivo by reducing the sequestration in remarkable magnitudes. In tumour-free mice, replication-deficient $Ad5_{NULL}$-A20 demonstrated significantly reduced viral transgene expression the liver, spleen and lungs compared to the parental Ad5 (Fig. 5), and lower viral genome copy number in all off-target organs relative to the Ad5 vector (Fig. 6).

To test efficacy of an oncolytic form of our de-targeted/re-targeted $Ad5_{NULL}$-A20 vector, we established an orthotopic i.p. xenograft model of human EOC SKOV3 in immunocompromised mice. The more localised bio-distribution of virally-encoded transgene expression of oncolytic $Ad5_{NULL}$-A20 following intraperitoneal administration was consistent with reduced off-target sequestration and/or tumour-selective virus uptake (Fig. 7B–E). This was supported by the superior survival of animals treated with $Ad5_{NULL}$-A20 relative to Ad5 in a SKOV3 xenograft model (Fig. 7E), although extended survival (compared to unmodified Ad5) was not observed in mice treated with the oncolytic Ad5.A20 variant. This observation highlights that efficacy in vivo depends upon both the combination of complete ablation of all native means of cellular uptake via hCAR, αvβ3/5 integrins and FX, coupled with an efficient

and selective retargeting mechanism to tumour-associated ligands, such as the αvβ6: A20 receptor: ligand interaction. This observation likely explains previous studies (51, 52) which described no improved efficacy (compared to oncolytic Ad5) of virotherapies targeted to αvβ6 integrin, since the vectors used in those studies lacked modifications in at least two of the three native infectious pathways (the hexon: FX and penton base: αvβ3/5 interactions). Additional studies will be needed to fully evaluate αvβ6+ cancer re-targeting in vivo, as well as to dissect the fate in tissues and immunological responses to the $Ad5_{NULL}$-A20 vector.

Local, i.p. $Ad5_{NULL}$-A20 administration presents a promising treatment option for advanced, chemotherapy-resistant, αvβ6+ ovarian cancer. Here, we describe a novel vector that can be further manipulated for various clinical applications, with the scope of selective targeting to αvβ6 integrin-expressing cells and minimal off-target effects that limit current Ad5-based therapies. $Ad5_{NULL}$-A20 vector provides an agile and versatile platform that could ultimately be modified for precision virotherapy applications by various innovative approaches, potentially providing a platform for the local, tumour selective over-expression of additional, virally encoding therapeutic modalities, such as immunotherapies.

ACKNOWLEDGEMENTS

We are most grateful to patients at Velindre Cancer Centre, Cardiff, UK, who donated ascites samples. We would like to thank Mrs Dawn Roberts for technical assistance, Dr Richard Stanton for his expertise in AdZ recombineering, Dr Alexander Greenshields-Watson for his assistance with homology modelling and structural biology, the team who maintain the YASARA energy minimisation server, Dr Edward Wang for his guidance in immunohistochemistry, Dr Lisa Spary and clinicians at Velindre Cancer Centre for access to clinical ascites samples, Mr William Matchett for his help with the IVIS 200 software, and Prof Gavin Wilkinson, Dr Michael Barry and Dr John Marshall for insightful discussions.

H.U-K was supported by a Cancer Research Wales PhD studentship to A.L.P., J. A. D is supported by a Cancer Research UK Biotherapeutics Drug Discovery Project Award to A.L.P. (project reference C52915/A23946). A.T.B is supported by a Tenovus Cancer Care PhD studentship to A.L.P. (project reference PhD2015/L13). A.L.P. is funded by Higher Education Funding Council for Wales.

FIGURE LEGENDS

Figure 1. Generated vectors. (A) Viral titres and expected tropisms of Ad5 and triply de-targeted, αvβ6 integrin re-targeted vector, $Ad5_{NULL}$-A20; (B) Vector map of the oncolytic $Ad5_{NULL}$-A20; (C) Homology modelling of the adenovirus serotype 5 fiber knob with A20 peptide (NAVPNLRGDLQVLAQKVART; dark blue) within the HI loop of fiber knob domain (Ad5.A20; in light blue) in complex with αv (green) and β6 (magenta) integrin subunits shows a potential mechanism for the $Ad5_{NULL}$-A20 interface. (D) Residues in both αv and β6 subunits form hydrogen bonds (red dashes), stabilising a charged interface (αvβ6, negative; A20, positive). Residues in Ad5s CD loop form further polar interactions. CAR, coxsackie and adenovirus receptor; FX, coagulation factor 10; HVR7, hypervariable region 7 (42); KO1, CAR-binding mutation in fiber knob AB loop (53); Luc, luciferase transgene; repl. def., replication-defective; vp, viral particle.

Figure 2. Ablation of native receptor tropisms. (A) Binding of replication-deficient Ad5 and $Ad5_{NULL}$-A20 vectors to coxsackie and adenovirus receptor (CAR). Ratio of viral transgene expression from $Ad5_{NULL}$-A20 relative to Ad5 is indicated above bars. (B) Binding of replication-deficient Ad5 and HVR7-mutated Ad5 variant (42) to coagulation factor 10 (FX) was assessed in luciferase assays by infecting CHO-K1 cells in the presence of human FX with (+) or without (–) anticoagulant X-bp. HVR7, FX-binding mutation. Statistical significance: ns, $p>0.05$; **, $p<0.01$.

Figure 3. In vitro assessment of αvβ6 integrin re-targeting. Transduction efficiency of replication-deficient wild-type (Ad5) and triply-detargeted, integrin re-targeted ($Ad5_{NULL}$-A20) vectors in (A) αvβ6+ BT-20 breast cancer cells and (B) αvβ6+ primary epithelial ovarian cancer (EOC) cells from patient 004. (C) Competition inhibition of αvβ6 integrin-mediated cell entry in SKOV3-β6 cells. The highest 10% αvβ6-expressing SKOV3-β6 cells were sorted by FACS, sub-cultured and infected. IgG, normal mouse IgG control; 10D5, anti-αvβ6 function-blocking antibody. Ratio of viral transgene expression is indicated above bars. Statistical significance: ns, $p>0.05$; *, $p<0.05$; **, $p<0.01$; ***, $p<0.001$; ****, $p<0.0001$.

Figure 4. The effect of malignant ovarian ascites on vector transduction ex vivo. (A) Quantification of anti-Ad5 antibodies in twenty clinical ovarian ascites (OAS) samples and control serum from a healthy male volunteer (solid black line) by ELISA. Horizontal lines indicate 50% and 100% binding of anti-Ad5 abs in the control serum. (B) Antigen specificity of anti-Ad5 antibodies in

ascites and serum by Western blot, using denatured whole virus particles. (C) Vector transduction efficiency of replication-defective (Ad5) and $Ad5_{NULL}$-A20 vectors, in the absence and presence of varying dilutions of ascites from an ovarian cancer patient 004 in primary ex vivo culture of epithelial ovarian cancer cells from patient 004. Cells were pre-incubated with ascending concentrations of ascites and infected.

Figure 5. Biodistribution of replication-defective vector infection at 72 h following systemic delivery in non-tumour-bearing animals. (A) Biodistribution study schedule and (B) in vivo imaging of biodistribution of replication-defective (Ad5) and triply de-targeted $Ad5_{NULL}$-A20 virus, 3 days after intravenous injection in the tail vein. Quantitation of total luminescence signal from panel B: in (C) whole body, (D) liver, (E) spleen, (F) lungs, (G) ovaries and (H) heart. i.p., intraperitoneal; IVIS, in vivo imaging system; p.i., post-infection; vp, viral particle. Error bars represent standard error of the mean; n=5/group; ns, $p>0.05$; *, $p<0.05$; **, $p<0.01$; ***, $p<0.001$; ****, $p<0.0001$.

Figure 6. Viral genome copy number in off-target organs at 72 hours following systemic delivery. Adenovirus genome copy number from tissues excised from animals in Fig. 5: (A) liver, (B) spleen, (C) lungs, (D) ovaries and (E) heart, as determined by qPCR for the hexon gene, following systemic vector delivery. Error bars represent standard error of the mean; n=5/group; ns, $p>0.05$; *, $p<0.05$; **, $p<0.01$; ***, $p<0.001$; ****, $p<0.0001$. Numbers below graphs indicate fold decrease of the $Ad5_{NULL}$-A20 group relative to the Ad5 group.

Figure 7. Oncolytic efficacy study: intraperitoneal delivery of oncolytic vectors in ovarian cancer xenograft model. (A) Study schedule. Intraperitoneal xenografts of human ovarian cancer SKOV3 cells were implanted into immune-compromised mice (n=5/group), then animals were treated with 3 doses of intravenous oncolytic Ad5, αvβ6 integrin re-targeted Ad5.A20 or triply de-targeted, αvβ6 integrin re-targeted $Ad5_{NULL}$-A20, on days 14, 16 and 18. (B) Luminescence heat map images and quantitation of total body luminescence were determined at 48 h after the first treatment (C; Day 16), and at 7 days after the first treatment (D; Day 21). (E) Overall survival of animals inoculated with SKOV3 xenografts (αvβ6-low/CAR+) and then treated with virus, as above, shown as a Kaplan–Meyer survival curve until the final study endpoint of 101 days. i.p., intraperitoneal; IVIS, in vivo imaging system; vp, viral particle *, $p<0.05$; **, $p<0.01$; ***, $p<0.001$. IVIS, In Vivo Imaging System.

REFERENCES

1. WCRF. Ovarian cancer statistics: World Cancer Research Fund International; 2012 [25/06/16]. Available from: http://www.wcrf.org/int/cancer-facts-figures/data-specific-cancers/ovarian-cancer-statistics.
2. Yeung TL, Leung CS, Yip KP, Au Yeung CL, Wong ST, Mok SC. Cellular and molecular processes in ovarian cancer metastasis. A Review in the Theme: Cell and Molecular Processes in Cancer Metastasis. Am J Physiol Cell Physiol. 2015;309(7):C444-56.
3. Koonings PP, Campbell K, Mishell Jr DR, Grimes DA. Relative frequency of primary ovarian neoplasms: A 10-year review. Obstetrics and Gynecology. 1989;74(6):921-6.
4. Koopman Van Aarsen LA, Leone DR, Ho S, Dolinski BM, McCoon PE, LePage DJ, et al. Antibody-mediated blockade of integrin αvβ 6 inhibits tumor progression in vivo by a transforming growth factor-β-regulated mechanism. Cancer Research. 2008;68(2):561-70.
5. Ahmed N, Riley C, Rice GE, Quinn MA, Baker MS. αvβ6 integrin-A marker for the malignant potential of epithelial ovarian cancer. Journal of Histochemistry and Cytochemistry. 2002;50(10):1371-9.
6. Bates RC, Bellovin DI, Brown C, Maynard E, Wu B, Kawakatsu H, et al. Transcriptional activation of integrin β6 during the epithelial-mesenchymal transition defines a novel prognostic indicator of aggressive colon carcinoma. Journal of Clinical Investigation. 2005;115(2):339-47.
7. Hazelbag S, Kenter GG, Gorter A, Dreef EJ, Koopman LA, Violette SM, et al. Overexpression of the αvβ6 integrin in cervical squamous cell carcinoma is a prognostic factor for decreased survival. Journal of Pathology. 2007;212(3):316-24.
8. Cantor DI, Cheruku HR, Nice EC, Baker MS. Integrin αvβ6 sets the stage for colorectal cancer metastasis. Cancer and Metastasis Reviews. 2015;34(4):715-34.
9. Weinacker A, Chen A, Agrez M, Cone RI, Nishimura S, Wayner E, et al. Role of the Integrin αvβ6 in Cell Attachment to Fibronectin: Heterologous expression of intact and secreted forms of the receptor. Journal of Biological Chemistry. 1994;269(9):6940-8.
10. Khan Z, Marshall JF. The role of integrins in TGFbeta activation in the tumour stroma. Cell Tissue Res. 2016;365(3):657-73.
11. FDA. FDA approves first-of-its-kind product for the treatment of melanoma: U.S. Food and Drug Administration; 2015 [Available from: http://www.fda.gov/NewsEvents/Newsroom/PressAnnouncements/ucm469571.htm.
12. Bourgeois-Daigneault MC, Roy DG, Aitken AS, El Sayes N, Martin NT, Varette O, et al. Neoadjuvant oncolytic virotherapy before surgery sensitizes triple-negative breast cancer to immune checkpoint therapy . Sci Transl Med. 2018;10(422):eaao1641.
13. Samson A, Scott KJ, Taggart D, West EJ, Wilson E, Nuovo GJ, et al. Intravenous delivery of oncolytic reovirus to brain tumor patients immunologically primes for subsequent checkpoint blockade. Sci Transl Med. 2018;10(422):eaam7577.
14. clinicaltrials.gov. clinicalTrials.gov: U.S. National Institutes of Health; 2016 [Available from: www.clinicaltrials.gov.
15. Bett AJ, Prevec L, Graham FL. Packaging capacity and stability of human adenovirus type 5 vectors. J Virol. 1993;67:5911-21.
16. Mast TC, Kierstead L, Gupta SB, Nikas AA, Kallas EG, Novitsky V, et al. International epidemiology of human pre-existing adenovirus (Ad) type-5, type-6, type-26 and type-36 neutralizing antibodies: Correlates of high Ad5 titers and implications for potential HIV vaccine trials. Vaccine. 2010;28(4):950-7.
17. Parker AL, Waddington SN, Nicol CG, Shayakhmetov DM, Buckley SM, Denby L, et al. Multiple vitamin K-dependent coagulation zymogens promote adenovirus-mediated gene delivery to hepatocytes. Blood. 2006;108(8):2554-61.
18. Uusi-Kerttula H, Hulin-Curtis S, Davies J, Parker AL. Oncolytic Adenovirus: Strategies and Insights for Vector Design and Immuno-Oncolytic Applications. Viruses. 2015;7(11):6009-42.
19. Waddington SN, McVey JH, Bhella D, Parker AL, Barker K, Atoda H, et al. Adenovirus Serotype 5 Hexon Mediates Liver Gene Transfer. Cell. 2008;132(3):397-409.
20. Bergelson JM, Cunningham JA, Droguett G, Kurt-Jones EA, Krithivas A, Hong JS, et al. Isolation of a common receptor for Coxsackie B viruses and adenoviruses 2 and 5. Science. 1997;275(5304):1320-3.
21. Coyne CB, Bergelson JM. CAR: A virus receptor within the tight junction. Advanced Drug Delivery Reviews. 2005;57(6):869-82.

22. Li Y, Pong RC, Bergelson JM, Hall MC, Sagalowsky AI, Tseng CP, et al. Loss of adenoviral receptor expression in human bladder cancer cells: A potential impact on the efficacy of gene therapy. Cancer Research. 1999;59(2):325-30.
23. Pearson AS, Koch PE, Atkinson N, Xiong M, Finberg RW, Roth JA, et al. Factors limiting adenovirus-mediated gene transfer into human lung and pancreatic cancer cell lines. Clin Cancer Res. 1999;5(12):4208-13.
24. Asaoka K, Tada M, Sawamura Y, Ikeda J, Abe H. Dependence of efficient adenoviral gene delivery in malignant glioma cells on the expression levels of the Coxsackievirus and adenovirus receptor. J Neurosurg. 2000;92(6):1002-8.
25. Kim JS, Lee SH, Cho YS, Choi JJ, Kim YH, Lee JH. Enhancement of the adenoviral sensitivity of human ovarian cancer cells by transient expression of coxsackievirus and adenovirus receptor (CAR). Gynecol Oncol. 2002;85(2):260-5.
26. Kim M, Zinn KR, Barnett BG, Sumerel LA, Krasnykh V, Curiel DT, et al. The therapeutic efficacy of adenoviral vectors for cancer gene therapy is limited by a low level of primary adenovirus receptors on tumour cells. Eur J Cancer. 2002;38(14):1917-26.
27. DiCara D, Rapisarda C, Sutcliffe JL, Violette SM, Weinreb PH, Hart IR, et al. Structure-function analysis of Arg-Gly-Asp helix motifs in αvβ6 integrin ligands. Journal of Biological Chemistry. 2007;282(13):9657-65.
28. Dicara D, Burman A, Clark S, Berryman S, Howard MJ, Hart IR, et al. Foot-and-mouth disease virus forms a highly stable, EDTA-resistant complex with its principal receptor, integrin alphavbeta6: implications for infectiousness. J Virol. 2008;82(3):1537-46.
29. Stanton RJ, McSharry BP, Armstrong M, Tomasec P, Wilkinson GWG. Re-engineering adenovirus vector systems to enable high-throughput analyses of gene function. BioTechniques. 2008;45(6):659-68.
30. Uusi-Kerttula H, Davies J, Coughlan L, Hulin-Curtis S, Jones R, Hanna L, et al. Pseudotyped alphavbeta6 integrin-targeted adenovirus vectors for ovarian cancer therapies. Oncotarget. 2016.
31. Uusi-Kerttula H, Legut M, Davies J, Jones R, Hudson E, Hanna L, et al. Incorporation of Peptides Targeting EGFR and FGFR1 into the Adenoviral Fiber Knob Domain and Their Evaluation as Targeted Cancer Therapies. Hum Gene Ther. 2015;26(5):320-9.
32. Fueyo J, Gomez-Manzano C, Alemany R, Lee PSY, McDonnell TJ, Mitlianga P, et al. A mutant oncolytic adenovirus targeting the Rb pathway produces anti-glioma effect in vivo. Oncogene. 2000;19(1):2-12.
33. Gros A, Martínez-Quintanilla J, Puig C, Guedan S, Molleví DG, Alemany R, et al. Bioselection of a gain of function mutation that enhances adenovirus 5 release and improves its antitumoral potency. Cancer Research. 2008;68(21):8928-37.
34. Xia D, Henry LJ, Gerard RD, Deisenhofer J. Crystal structure of the receptor-binding domain of adenovirus type 5 fiber protein at 1.7 Å resolution. Structure. 1994;2(12):1259-70.
35. Kotecha A WQ, Dong X, et al. . *Nature Communications* . 2017, doi:10.1038/ncomms15408. Rules of engagement between αvβ6 integrin and foot-and-mouth disease virus.
36. Emsley P, Lohkamp B, Scott WG, Cowtan K. Features and development of *Coot*. Acta Crystallogr D Biol Crystallogr. 2010;66:486-501.
37. Schrödinger L. The PyMOL Molecular Graphics System. 2.0 ed.
38. Krieger E, Koraimann G, Vriend G. Increasing the precision of comparative models with YASARA NOVA—a self-parameterizing force field. 2002;47:393–402.
39. Krissinel E, Henrick K. Inference of macromolecular assemblies from crystalline state. J Mol Biol. 2007;372:774-97.
40. Hynes RO. Integrins: bidirectional, allosteric signaling machines. Cell. 2002;110(6):673-87.
41. Stallwood Y, Fisher KD, Gallimore PH, Mautner V. Neutralisation of adenovirus infectivity by ascitic fluid from ovarian cancer patients. Gene Therapy. 2000;7(8):637-43.
42. Alba R, Bradshaw AC, Parker AL, Bhella D, Waddington SN, Nicklin SA, et al. Identification of coagulation factor (F)X binding sites on the adenovirus serotype 5 hexon: Effect of mutagenesis on FX interactions and gene transfer. Blood. 2009;114(5):965-71.
43. Allen MD, Thomas GJ, Clark S, Dawoud MM, Vallath S, Payne SJ, et al. Altered microenvironment promotes progression of preinvasive breast cancer: Myoepithelial expression of avb6 integrin in DCIS identifies high-risk patients and predicts recurrence. Clinical Cancer Research. 2014;20(2):344-57.
44. Hausner SH, Abbey CK, Bold RJ, Gagnon MK, Marik J, Marshall JF, et al. Targeted in vivo imaging of integrin alphavbeta6 with an improved radiotracer and its relevance in a pancreatic tumor model. Cancer Res. 2009;69(14):5843-50.

45. Kogelberg H, Tolner B, Thomas GJ, Di Cara D, Minogue S, Ramesh B, et al. Engineering a single-chain Fv antibody to alpha v beta 6 integrin using the specificity-determining loop of a foot-and-mouth disease virus. J Mol Biol. 2008;382(2):385-401.
46. Whilding LM, Vallath S, Maher J. The integrin alphavbeta6: a novel target for CAR T-cell immunotherapy? Biochem Soc Trans. 2016;44(2):349-55.
47. Moore KM, Thomas GJ, Duffy SW, Warwick J, Gabe R, Chou P, et al. Therapeutic Targeting of Integrin αvβ6 in Breast Cancer. JNCI: Journal of the National Cancer Institute. 2014;106(8):dju169-dju.
48. D'Souza SE, Ginsberg MH, Plow EF. Arginyl-glycyl-aspartic acid (RGD): a cell adhesion motif. Trends Biochem Sci. 1991;16(7):246-50.
49. Blackwell JL, Hui L, Gomez-Navarro J, Dmitriev I, Krasnykh V, Richter CA, et al. Using a tropism-modified adenoviral vector to circumvent inhibitory factors in ascites fluid. Human Gene Therapy. 2000;11(12):1657-69.
50. Hemminki A, Wang M, Desmond RA, Strong TV, Alvarez RD, Curiel DT. Serum and ascites neutralizing antibodies in ovarian cancer patients treated with intraperitoneal adenoviral gene therapy. Human Gene Therapy. 2002;13(12):1505-14.
51. Man YKS, Davies JA, Coughlan L, Pantelidou C, Blazquez-Moreno A, Marshall JF, et al. The Novel Oncolytic Adenoviral Mutant Ad5-3Delta-A20T Retargeted to alphavbeta6 Integrins Efficiently Eliminates Pancreatic Cancer Cells. Mol Cancer Ther. 2018;17(2):575-87.
52. Coughlan L, Vallath S, Gros A, Gimenez-Alejandre M, Van Rooijen N, Thomas GJ, et al. Combined fiber modifications both to target alpha(v)beta(6) and detarget the coxsackievirus-adenovirus receptor improve virus toxicity profiles in vivo but fail to improve antitumoral efficacy relative to adenovirus serotype 5. Hum Gene Ther. 2012;23(9):960-79.
53. Smith T, Idamakanti N, Kylefjord H, Rollence M, King L, Kaloss M, et al. In vivo hepatic adenoviral gene delivery occurs independently of the coxsackievirus-adenovirus receptor. Molecular Therapy. 2002;5(6):770-9.

Figure 1

A

	Titre (vp/mL)		Receptor binding			
Vector	Repl. def.	Oncolytic	αvβ3/5	αvβ6	CAR	FX
Ad5	3.9×10^{12}	1.1×10^{12}	+	–	+	+
Ad5.A20	5.5×10^{12}	2.2×10^{12}	+	+	+	+
$Ad5_{NULL}$-A20	3.0×10^{12}	1.5×10^{12}	–	+	–	–

B

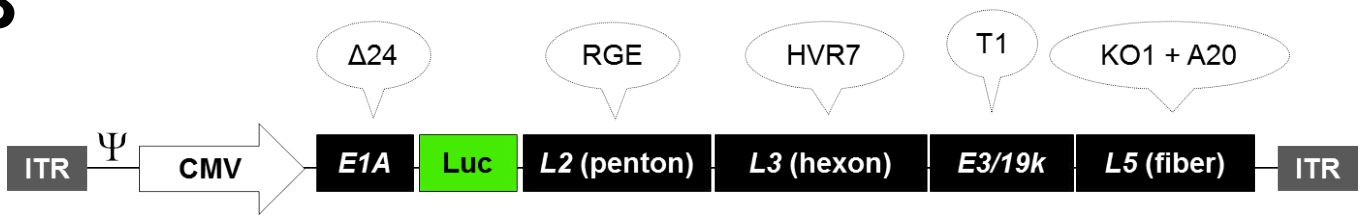

C

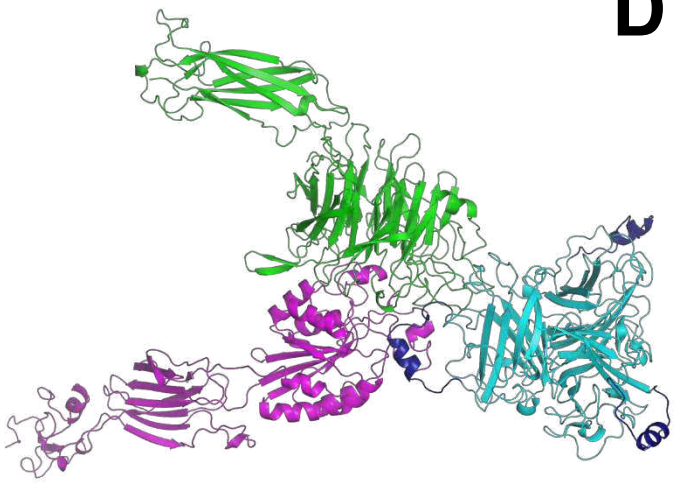

D

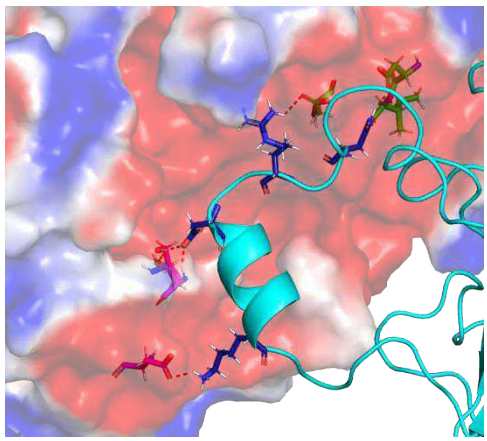

Figure 2

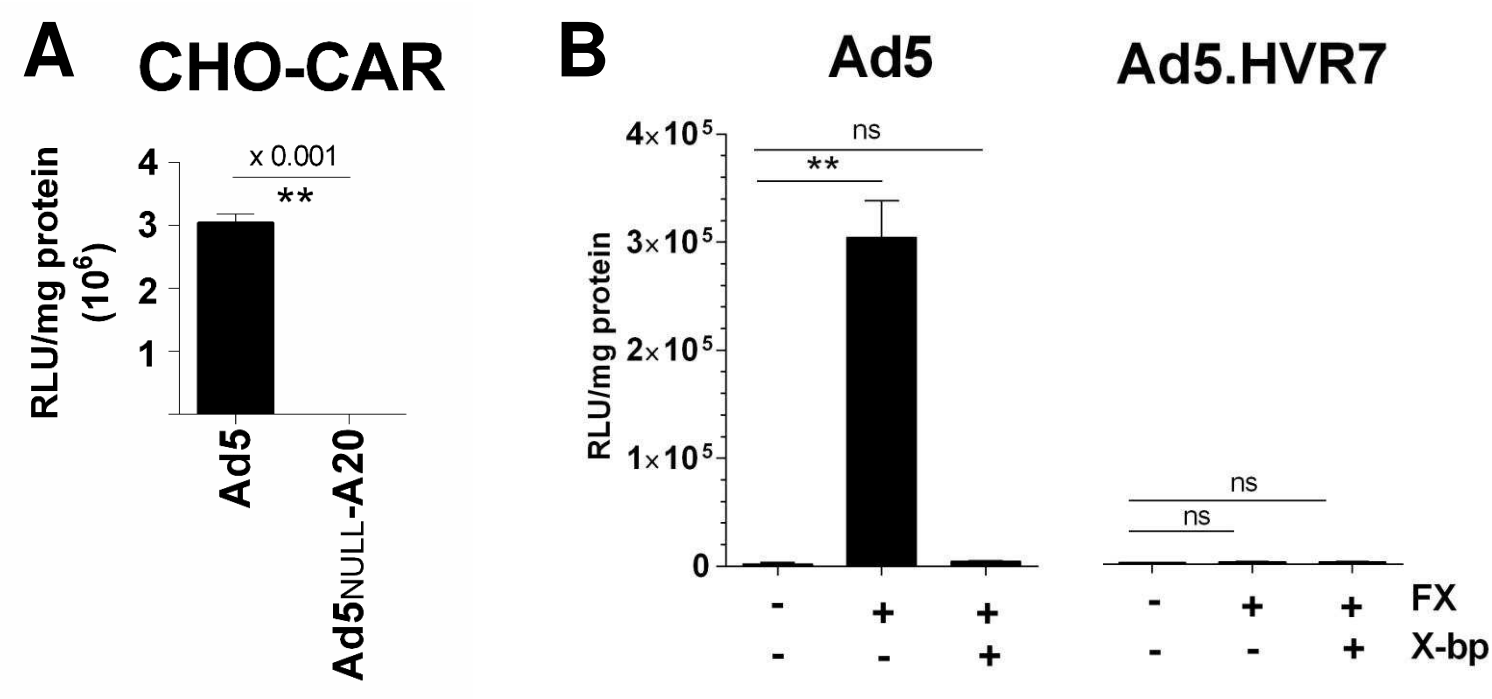
A
CHO-CAR
RLU/mg protein (10^6)
4
3
2
1
x 0.001
**
Ad5
Ad5NULL-A20
B
Ad5
Ad5.HVR7
4×10^5
3×10^5
2×10^5
1×10^5
0
RLU/mg protein
ns
**
ns
ns
FX
X-bp

Figure 3

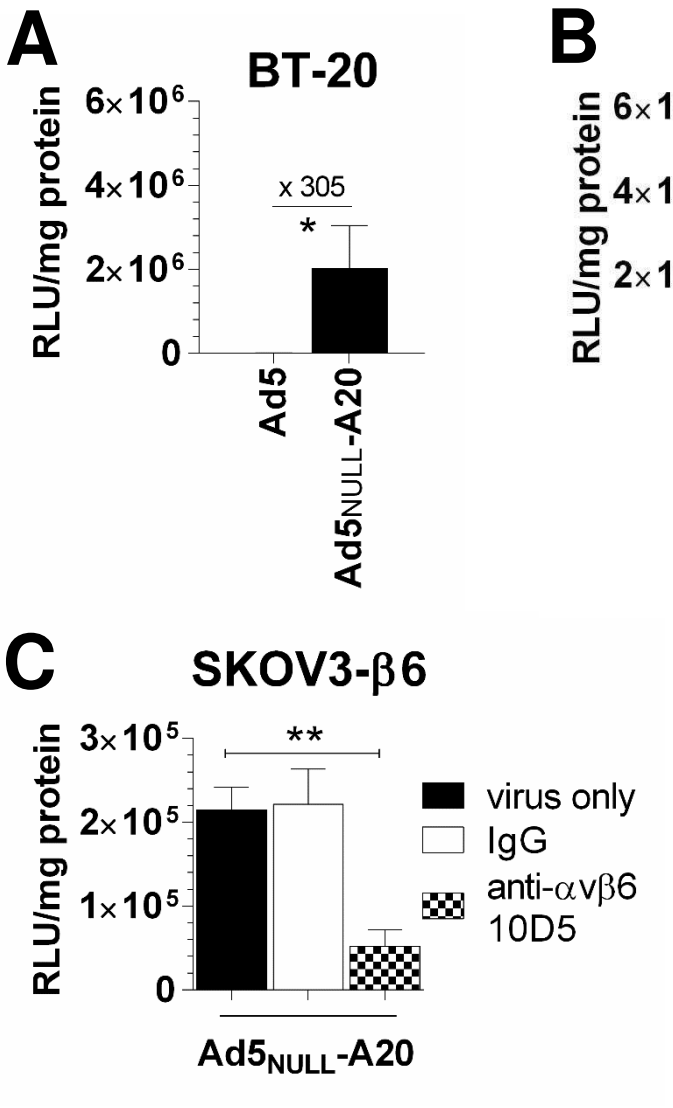
A
BT-20
RLU/mg protein
6×10^6
4×10^6
2×10^6
0
x 305
*
Ad5
Ad5NULL-A20
B
EOC004
RLU/mg protein
6×10^6
4×10^6
2×10^6
0
x 69
**
Ad5
Ad5NULL-A20
C
SKOV3-β6
RLU/mg protein
3×10^5
2×10^5
1×10^5
0
**
virus only
IgG
anti-αvβ6
10D5
Ad5NULL-A20

Figure 4

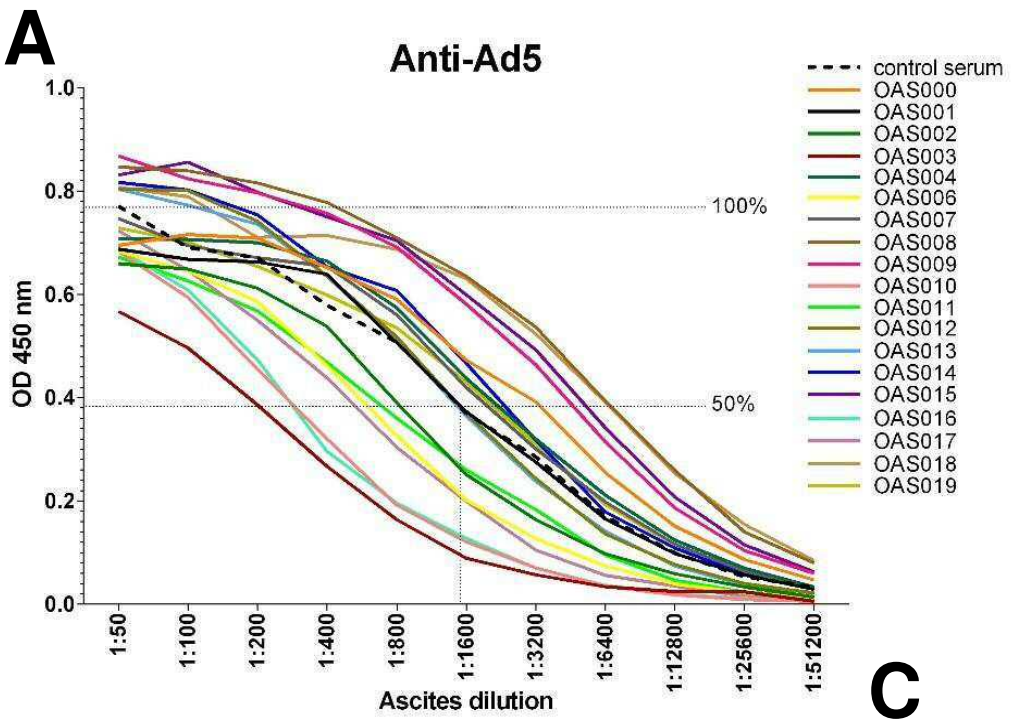
A
Anti-Ad5
control serum
OAS000
OAS001
OAS002
OAS003
OAS004
OAS006
OAS007
OAS008
OAS009
OAS010
OAS011
OAS012
OAS013
OAS014
OAS015
OAS016
OAS017
OAS018
OAS019
100%
50%
OD 450 nm
1.0
0.8
0.6
0.4
0.2
0.0
1:50
1:100
1:200
1:400
1:800
1:1600
1:3200
1:6400
1:12800
1:25600
1:51200
Ascites dilution

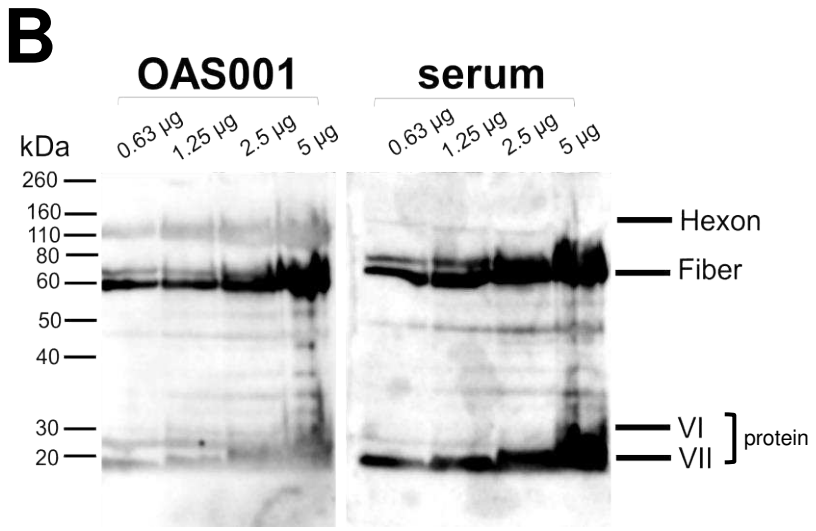
B
OAS001
serum
kDa
0.63 µg
1.25 µg
2.5 µg
5 µg
0.63 µg
1.25 µg
2.5 µg
5 µg
260
160
110
80
60
50
40
30
20
Hexon
Fiber
VI
VII
protein

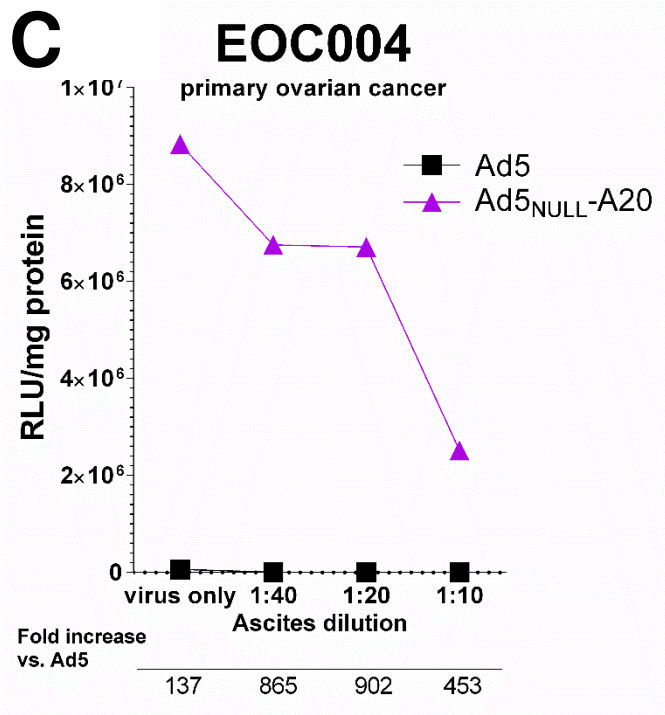
C
EOC004
primary ovarian cancer
Ad5
Ad5NULL-A20
RLU/mg protein
8×10⁶
6×10⁶
4×10⁶
2×10⁶
0
virus only
1:40
1:20
1:10
Ascites dilution
Fold increase
vs. Ad5
137
865
902
453

Figure 5

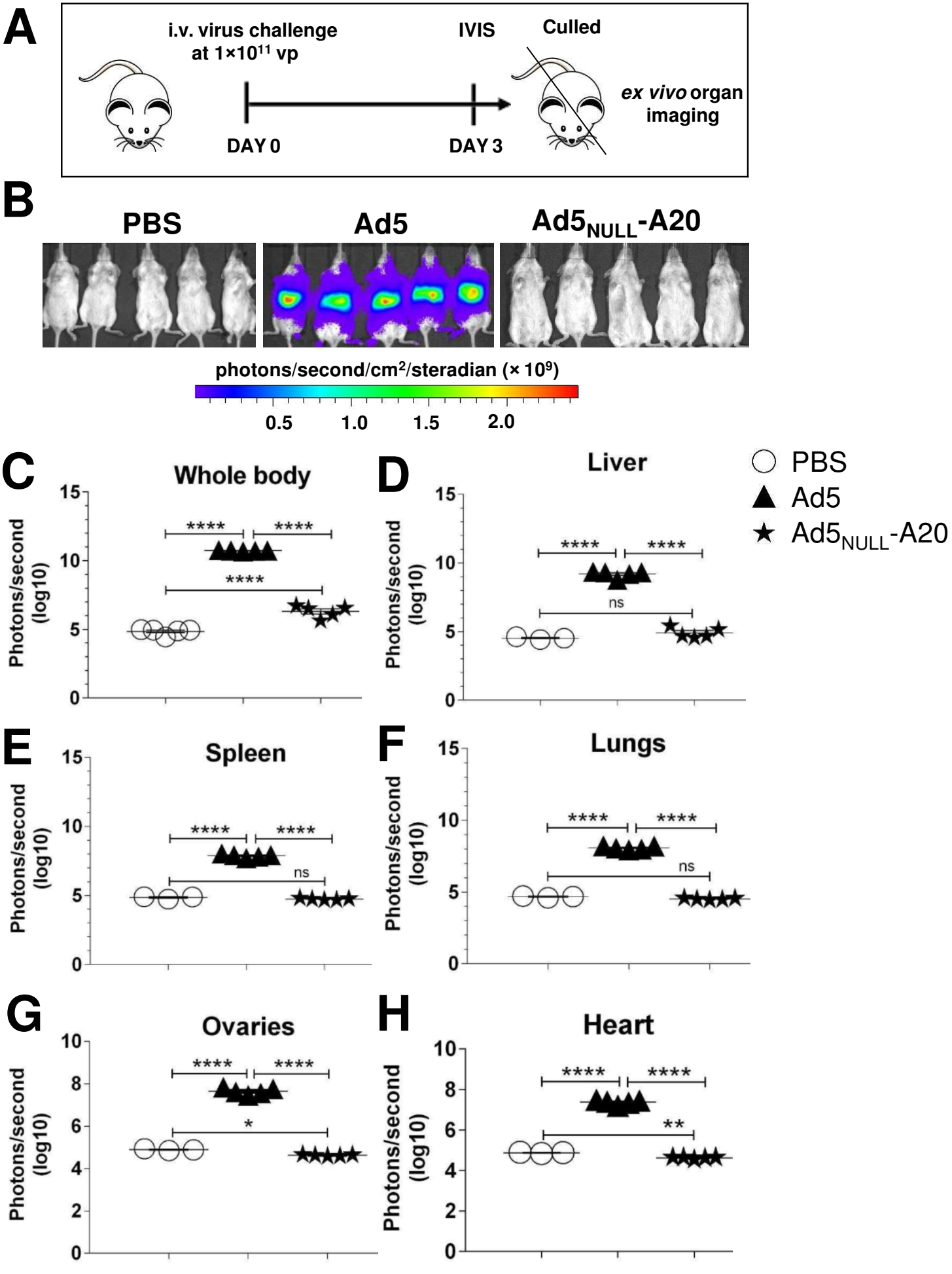
A
i.v. virus challenge at 1×10^11 vp
IVIS
Culled
ex vivo organ imaging
DAY 0
DAY 3
B
PBS
Ad5
Ad5NULL-A20
photons/second/cm2/steradian (× 10^9)
0.5
1.0
1.5
2.0
C
Whole body
D
Liver
E
Spleen
F
Lungs
G
Ovaries
H
Heart
Photons/second (log10)
PBS
Ad5
Ad5NULL-A20
****
ns
*
**

Figure 6

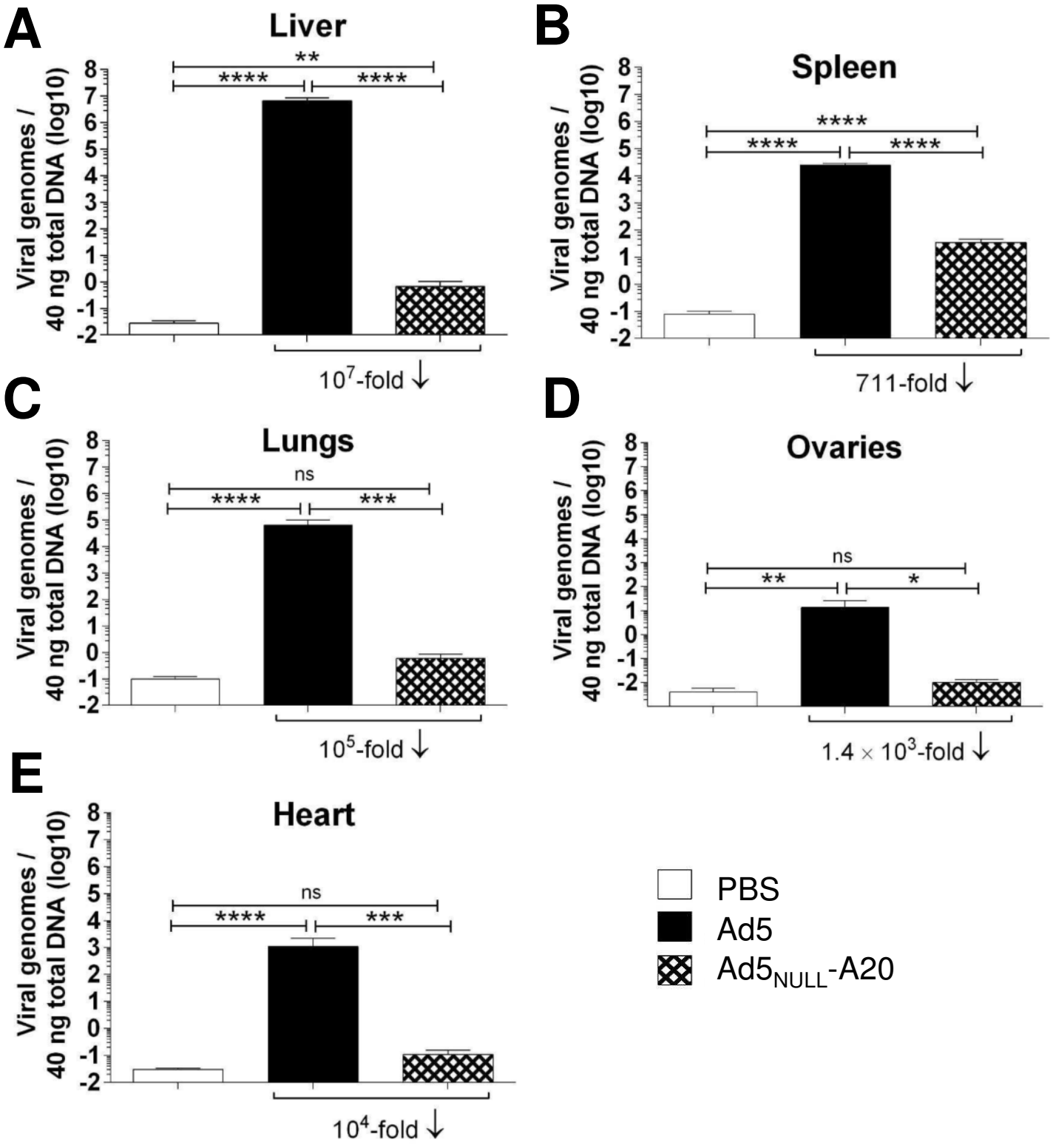
A
Liver
Viral genomes / 40 ng total DNA (log10)
**
****
****
10^7-fold ↓
B
Spleen
****
****
****
711-fold ↓
C
Lungs
ns
****
***
10^5-fold ↓
D
Ovaries
ns
**
*
1.4 × 10^3-fold ↓
E
Heart
ns
****
***
10^4-fold ↓
PBS
Ad5
Ad5NULL-A20

Figure 7

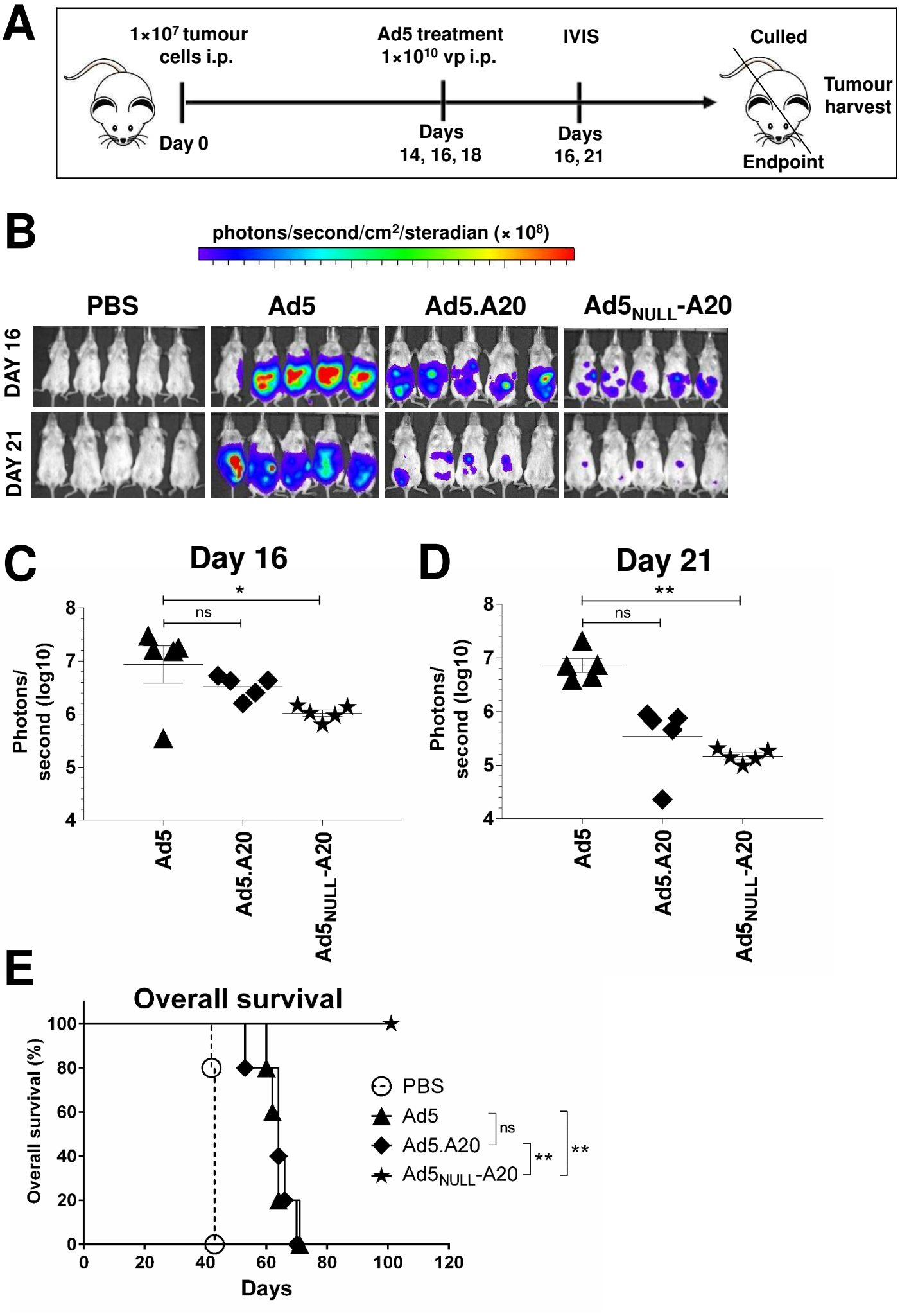
A
1×10^7 tumour cells i.p.
Day 0
Ad5 treatment 1×10^10 vp i.p.
Days 14, 16, 18
IVIS
Days 16, 21
Culled
Tumour harvest
Endpoint
B
photons/second/cm^2/steradian (× 10^8)
PBS
Ad5
Ad5.A20
Ad5NULL-A20
DAY 16
DAY 21
C
Day 16
Photons/ second (log10)
ns
*
Ad5
Ad5.A20
Ad5NULL-A20
D
Day 21
Photons/ second (log10)
ns
**
Ad5
Ad5.A20
Ad5NULL-A20
E
Overall survival
Overall survival (%)
Days
PBS
Ad5
Ad5.A20
Ad5NULL-A20
ns
**
**